

Theoretical spin transport analysis for a spin pseudovalve-type L_j /semiconductor/ L_j trilayer (with $L_j = \text{ferromagnetic}$)

Julián A. Zúñiga* and Arles V. Gil Rebaza†

Instituto de Física La Plata CONICET, Universidad Nacional de La Plata, La Plata 1900. Argentina

Diego F. Coral Coral

Departamento de Física, Universidad del Cauca, Popayán 190002. Colombia

(Dated: September 10, 2024)

In this work, a theoretical study of spin transport in a pseudovalve spin (PSV) heterostructure is conducted. For the semiconductor (SC), the conduction band at the Γ point of reciprocal space and spin-orbit coupling (SOC) are considered. For the ferromagnetic (FM) electrodes on the left (l) and right (r), the internal exchange energy (Δ_j , where $j = (l, r)$) and the magnetization normal vector (\mathbf{n}_j) on the barrier plane are taken into account. An analytical expression for the transmission probability as a function of \mathbf{n}_j direction was obtained from the *Schrödinger-Pauli* equations with the boundary conditions. Furthermore, the tunnel magnetoresistance (TMR) at $T \approx 0$ K was calculated, depending on the direction of the crystallographic axis favoring the magnetization (θ_m) of the FM and the thickness of the SC, using the *Landauer-Büttiker* formula for a single channel. It is observed that the TMR reaches its maximum value when the \mathbf{n}_l direction is parallel to θ_m . Applying this physico-mathematical model to the Fe/SC/Fe PSV, with SC as GaAs, GaSb, and InAs, it was found that the *Dresselhaus* SOC does not significantly contribute to the TMR.

I. INTRODUCTION

The pseudovalve spin (PSV) heterostructure, formed by electrode/insulator/electrode, where the electrodes used are ferromagnetic metals, magnetically diluted semiconductors (DMS), or ferromagnetic semiconductors (FMS), have attracted great interest as elements in spintronic devices due to their magnetoresistances (MR), which have been extensively studied [1–4]. In particular, if the magnetic insulator is a semiconductor (SC), a heterostructure with a magnetic tunnel junction (MTJ) is obtained. Therefore, the tunnel magnetoresistance (TMR) is estimated [5–8] using the *Landauer-Büttiker* formula, in this case for a channel at $T \approx 0$ K, which allows for a description of electronic transport in mesoscopic systems [9].

For theoretical calculation of the transmission probability, some authors such as *J. C. Slonczewski* [10] and *Yunong Qi* et al. [11] have implemented the two-band model, which is related to the *Fermi* energy and the internal exchange energy (Δ_j , where $j = (l, r)$) of the ferromagnetic (FM) layers. They set the molecular field in the first FM layer parallel to the crystallographic axis [010], while the field of the second FM layer moves in the (100) plane, with rectangular and delta *Dirac* potential barriers, respectively. The model eventually variations, such as in the description of Δ_j , by substituting the molecular field with a relation between its magnitude and the *Zeeman* spin splitting energy [5, 7, 8]. Additionally, it presents the *Pauli* spin operator [5, 7, 12, 13] as

the scalar product between the magnetization direction vector and the Pauli's matrices [6, 14, 15], generating a system of *Schrödinger-Pauli* equations. On the other hand, it can be observed that the rotation spinor is frequently used to diagonalize the Hamiltonians involved in the two-band model [5, 6, 10, 11], but the work of *A. Matos* et al. [14] proposes a spinor that related with the direction \mathbf{n}_l and the one formed between \mathbf{n}_l and \mathbf{n}_r . This makes it possible for the axis along which the parallel and antiparallel configurations are defined to rotate to the crystallographic axis that favors magnetization.

Therefore, this work presents a physico-mathematical model where the majority spin channel and the wave vector of layer L_l are parallel to \mathbf{n}_l , as a particular case of the theory developed by *J. E. Bunder* [6], but following the formalism of *A. Matos* et al. [14] to define the spinors. Hence, the solution to the system of *Schrödinger-Pauli* equations is obtained. With boundary conditions, an analytical expression for the transmission probability is determined as a function of the direction of the normal vectors of magnetization located in the barrier plane, the thickness of the SC, and the *Dresselhaus* and *Rashba* spin-orbit coupling (SOC). The TMR is analyzed for a fixed direction of the crystallographic axis that favors magnetization (θ_m); considering the trilayer Fe/SC/Fe-type pseudovalves spin (PSVs), where the semiconductors (SCs) are GaAs, InAs, and GaSb. For the particular case presented by *K. Kondo* [15], there one not correspondence in the analyses for the aforementioned PSVs.

* jzuniga@iflp.unlp.edu.ar

† arlesv@fisica.unlp.edu.ar; Also at Departamento de Física, UNLP

II. THEORETICAL MODEL

The study of spin electronic transmission is done under the assumptions that the potential energy profile is a thin rectangular barrier (1-5 nm) with a height V_0 , such that $E_g/2 \leq V_0 < E_g$ where E_g is the band gap of the semiconductor [16] (see Fig. 1), the tunneling direction is parallel to the z axis, and that the wave vector on the barrier plane (\vec{k}_{\parallel}) is conserved throughout the heterostructure, allowing the decoupling of motion along the z axis from the other spatial degrees of freedom.

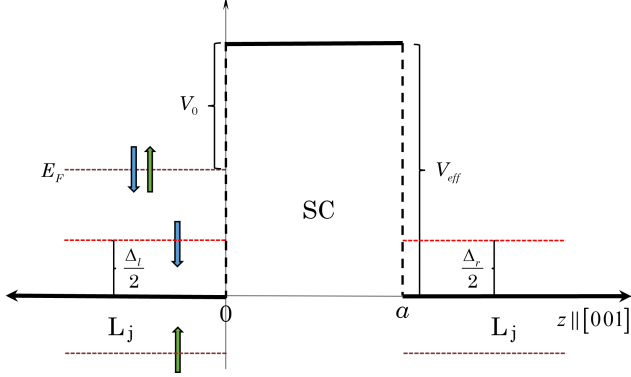


FIG. 1. Schematic representation of a rectangular quantum potential barrier for a two-band model in the growth direction of the heterostructure $[001]$, of height V_{eff} and thickness a , where E_F is the Fermi energy corresponding to the energy applied to the electron and Δ_j is the internal exchange energy [6, 14].

A. Description of the hamiltonians

The Hamiltonian for the regions $z < 0$ and $z > a$, corresponding to the L_l and L_r layers, respectively, is defined as [6, 14]:

$$\hat{\mathcal{H}}_j = \left[\frac{\hbar^2}{2m_j^*} (k_{z,j}^2 + k_{\parallel,j}^2) \right] \hat{\mathbb{I}} - \frac{\Delta_j}{2} \mathbf{n}_j \cdot \boldsymbol{\tau}, \quad (1)$$

where \hbar is the reduced Planck constant, m_j^* is the effective mass in layer L_j , $k_{\epsilon,j}$ with $\epsilon = (x, y, z)$ is an operator defined as $k_{\epsilon,j} = -i\partial_{\epsilon}$, and $k_{\parallel,j} = (k_{x,j}, k_{y,j})$ is the magnitude of the wave vector on the barrier plane. $\hat{\mathbb{I}}$ represents the identity matrix (2×2), and $\boldsymbol{\tau} = (\hat{\tau}_x, \hat{\tau}_y, \hat{\tau}_z)$ is the vector of Pauli matrices. The magnetization normal vector on the barrier plane is given by $\mathbf{n}_j = (\sin \theta_j, \cos \theta_j, 0)$.

The Hamiltonian with SOC for the region $0 < z < a$ is described as [17]:

$$\hat{\mathcal{H}}_{\sigma}^s = \left(\frac{\hbar^2}{2m_b^*} k_{\sigma}^2 + V_{eff} \right) \hat{\mathbb{I}} + \gamma (\hat{\tau}_y k_{y\sigma} - \hat{\tau}_x k_{x\sigma}) k_{z\sigma}^2 + \alpha (\hat{\tau}_x k_{y\sigma} - \hat{\tau}_y k_{x\sigma}), \quad (2)$$

where σ denotes whether the spin $\mathbf{S}_{\sigma}^{\pm}$ is parallel ($\sigma = \uparrow$ or 1) or antiparallel ($\sigma = \downarrow$ or -1) to \mathbf{n}_l (see Fig. 2), m_b^* is the effective mass in the SC, k_{σ} is the electron's wave vector in the barrier, and $V_{eff} = V_0 + E_F$, with E_F as the Fermi energy (see Fig. 1). Finally, γ and α are the Dresselhaus and Rashba SOC constants, respectively.

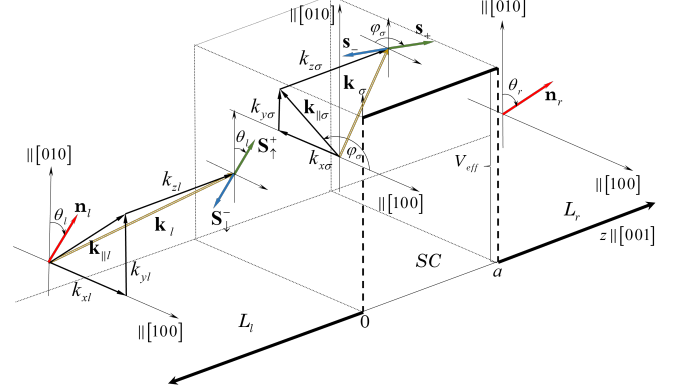


FIG. 2. Schematic representation of the magnetization normal vectors, \mathbf{n}_j , on the barrier plane related to the spin $\mathbf{S}_{\sigma}^{\pm}$ of layer L_l . Additionally, $\mathbf{k}_j = (k_{\parallel,j}, k_{z,j})$ are the wave vectors of the electron when it incident on the barrier for $j = l$ and similarly when it is transmitted $j = r$. Inside the barrier, the spin states of the SOC are represented (\mathbf{s}_{\pm}).

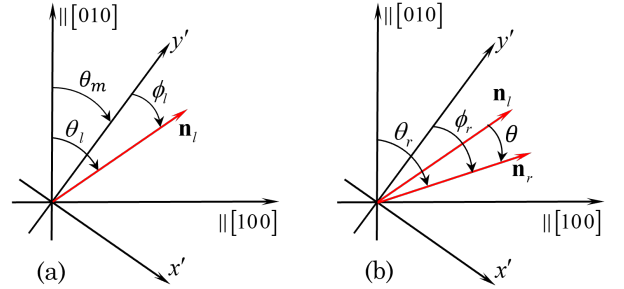


FIG. 3. Schematic representation of \mathbf{n}_j in the $x-y$ and $x'-y'$ planes. Where θ_m is the direction of the crystallographic axis favoring magnetization and $\theta = \phi_r - \phi_l$.

Considering Fig. 3 to define the spinor that diagonalizes the Hamiltonian $\hat{\mathcal{H}}_j$, we have:

$$|\chi_{\sigma}^j\rangle = \frac{1}{\sqrt{2}} \begin{pmatrix} 1 \\ i\sigma e^{-2\phi_l i} \end{pmatrix}, \quad (3)$$

where $\phi_l = \theta_l - \theta_m$.

Consequently, the energy eigenvalues for the layers L_j are described by the expression:

$$E_{\sigma}^j = \frac{\hbar^2}{2m_j^*} k_j^2 - \sigma \frac{\Delta_j}{2} \cos(\phi_l - \delta_j \theta), \quad (4)$$

with

$$\delta_j = \begin{cases} 0 & \text{if } j = l \\ 1 & \text{if } j = r \end{cases},$$

where θ represents the angle between \mathbf{n}_l and \mathbf{n}_r . while, the Hamiltonian $\hat{\mathcal{H}}_\sigma^s$ has energy eigenvalues,

$$E_\sigma^s = \frac{\hbar^2}{2m_b^*} k_\sigma^2 + V_{eff} + s\gamma k_\parallel k_{z\sigma}^2 + s\alpha k_{\parallel\sigma} \sin(2\phi_l), \quad (5)$$

with $s = \pm$, which represent the spin states. For the spin up “+” and the spin down “-” given the SOC. Where the spinor that diagonalizes the aforementioned Hamiltonian is [18]

$$|\chi_\sigma^s\rangle = \frac{1}{\sqrt{2}} \begin{pmatrix} 1 \\ -s e^{-i\varphi_\sigma^s} \end{pmatrix}, \quad (6)$$

where φ_σ^s is related to the direction of \mathbf{n}_l by the expression $\varphi_\sigma^s = \phi_l + s\sigma\frac{\pi}{2}$ (see Fig. 4).

B. Solution of Schrödinger-Pauli equation

The *Schrödinger-Pauli* equation, $\hat{\mathcal{H}}|\psi\rangle = E|\psi\rangle$, where $\hat{\mathcal{H}}$ is defined in terms of the step function $\Theta(z)$ as:

$$\hat{\mathcal{H}} = \hat{\mathcal{H}}_l\Theta(-z) + \hat{\mathcal{H}}_\sigma^s\Theta(z)\Theta(a-z) + \hat{\mathcal{H}}_r\Theta(z-a), \quad (7)$$

whose solution can be decoupled into a plane wave in the direction k_\parallel modulated by a wave function $|\phi_\sigma(z)\rangle = u_\sigma(z)|\chi\rangle$, which is the product of a periodic function and its respective spinor ($|\chi\rangle$). That is, $|\psi\rangle = e^{i\mathbf{k}_\parallel \cdot \mathbf{r}(x,y)} u_\sigma(z)|\chi\rangle$, where $\mathbf{r}(x,y)$ is a vector on the barrier plane that is parallel to the (001) plane (see Fig. 2). Then, $|\phi_\sigma(z)\rangle$ is determined by the following expression:

$$\begin{cases} \frac{1}{2\sqrt{k_\sigma^l}} e^{ik_\sigma^l z} |\chi_\sigma^l\rangle + \mathcal{R}_\sigma e^{-ik_\sigma^l z} |\chi_\sigma^l\rangle & \text{if } z < 0 \\ \sum_{s=\pm} \{(\mathcal{C}_\sigma^s e^{i\rho_s z} + \mathcal{D}_\sigma^s e^{-i\rho_s z}) |\chi_\sigma^s\rangle\} & \text{if } 0 < z < a, \\ \mathcal{T}_\sigma e^{ik_\sigma^r z} |\chi_\sigma^r\rangle & \text{if } z > a \end{cases} \quad (8)$$

where k_σ^j and ρ_s represent the magnitude of the wave vectors for the spins in the layers L_j and within the barrier, respectively. Consequently,

$$k_\sigma^j(\theta, k_{\parallel j}) = \sqrt{\frac{2m_j^*}{\hbar^2} \left(E_F + \sigma \frac{\Delta_j}{2} \cos(\phi_l - \delta_j \theta) \right) - k_{\parallel j}^2}, \quad (9)$$

$$\rho_s(\phi_l, k_\parallel) = \sqrt{\frac{2m_b^*}{\hbar^2} (V_{eff} - E_F) + k_\parallel^2 + s \frac{2m_b^* \alpha}{\hbar^2} k_\parallel \sin(2\phi_l)} \quad (10)$$

where E_F corresponds to layer L_j .

C. Transmission probability and TMR

The coefficients \mathcal{R}_σ , \mathcal{C}_σ^s , \mathcal{D}_σ^s , and \mathcal{T}_σ in equation (8) are determined applying boundary conditions at $z_l = 0$ and $z_r = a$. That is,

$$\begin{aligned} |\phi_\sigma^j(z_j)\rangle &= |\phi_\sigma^s(z_j)\rangle \\ \frac{1}{m_j^*} \partial_z |\phi_\sigma^j(z)\rangle \Big|_{z=z_j} &= \frac{1}{m_b^*} \partial_z |\phi_\sigma^s(z)\rangle \Big|_{z=z_j} \end{aligned} \quad (11)$$

Then, by the expression:

$$\Lambda_s^\pm = \frac{1}{2i\sqrt{k_\sigma^l}} \frac{\kappa_l(\rho_s \pm \kappa_r)}{(\kappa_l + \kappa_r)\rho_s \beta_\sigma^s} e^{-i(\frac{1}{2}\phi_l \pm \rho_s a)} \cos\left(\frac{1}{2}\phi_l\right), \quad (12)$$

where $\beta_\sigma^s = \cosh(\rho_s a) - i \frac{\kappa_l \kappa_r - \rho_s^2}{(\kappa_l + \kappa_r)\rho_s} \sinh(\rho_s a)$ and

$\kappa_j = \frac{m_b^*}{m_j^*} k_\sigma^j(\theta, k_{\parallel j})$, it is reached that $\mathcal{C}_\sigma^s = \Lambda_s^+$ and $\mathcal{D}_\sigma^s = \Lambda_s^-$. which implies that the transmission coefficient is determined by the expression:

$$\mathcal{T}_\sigma = \frac{1}{i\sqrt{k_\sigma^l}} \frac{\kappa_l}{\kappa_l + \kappa_r} e^{-i(k_\sigma^r a - \frac{1}{2}\phi_l)} \cos\left(\frac{1}{2}\phi_l\right) \sum_{s=\pm} (\beta_\sigma^s)^{-1}. \quad (13)$$

Consequently, the expression obtained for the transmission probability is:

$$\mathbb{T}_{\theta_l}^\sigma(k_{\parallel j}, \theta) = \frac{\kappa_l \kappa_r}{(\kappa_l + \kappa_r)^2} \cos^2\left(\frac{1}{2}\phi_l\right) \left| \sum_{s=\pm} (\beta_\sigma^s)^{-1} \right|^2. \quad (14)$$

The TMR = $(G_P - G_{AP})/G_{AP}$, where the conductance G_P occurs when $\mathbf{n}_l \parallel \mathbf{n}_r$ and the conductance G_{AP} occurs when $\mathbf{n}_l \not\parallel \mathbf{n}_r$. According to the *Landauer-Büttiker* formula for $T \approx 0$ K [19]

$$G_\ell = \frac{e^2 A_c}{(2\pi)^3 \hbar} \int_{k_1}^{k_2} dk_{\parallel j} \mathbb{T}(k_{\parallel j}, \theta), \quad (15)$$

where $\ell = P$ if $\theta = 0$ and for $\ell = AP$, $\theta = \pi$; A_c is the cross-section area of the junction, and $\mathbb{T}(k_{\parallel j}, \theta) = \mathbb{T}_{\theta_l}^\uparrow(k_{\parallel j}, \theta) + \mathbb{T}_{\theta_l}^\downarrow(k_{\parallel j}, \theta)$ is the transmittance coefficient. It should be noted that the expression (15) for $T = 0$ K, the *Landauer-Büttiker* formula has an approximation (LBA) defined by the expression [15, 20]:

$$G_\ell^v = \frac{e^2}{\pi \hbar} \mathbb{T}(k_{\parallel j}, \theta). \quad (16)$$

This latter will be considered to make comparisons with *K. Kondo* work [15].

III. RESULTS AND DISCUSSIONS

The TMR for this work is analyzed considering the PSV: Fe/SC/Fe at $T \approx 0$ K, with $k_{\parallel j} = k_\parallel$ and $k_1 = 0.1$

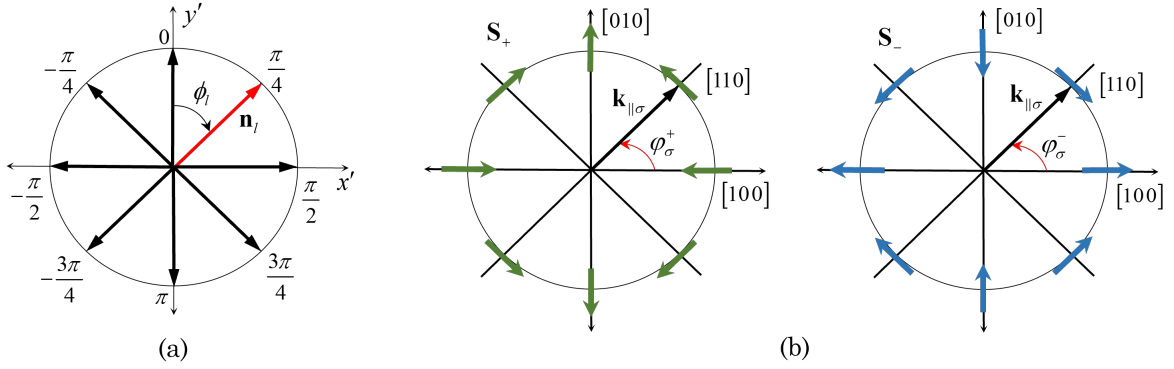


FIG. 4. Schematic representation of the relationship between the direction of the vectors (a) \mathbf{n}_l in the $x'-y'$ plane and (b) $\mathbf{k}_{\parallel\sigma}$ associated with the SOC *Dresselhaus* and *Rashba* spin states [18] (φ_{σ}^s with $s = \pm$).

nm^{-1} up to $k_2 = 0.4 \text{ nm}^{-1}$; for Fe, $m_j^* = m_e$ (electron mass), $\theta_m = \pi/4$ [14], $\Delta_j = 3.46 \text{ eV}$, and $E_F = 2.48 \text{ eV}$ [21]. The SOC constants for zinc-blende type SCs (III-V): GaAs, GaSb, and InAs are described in Table I, and the barrier height (V_0) of the SCs is 0.75 eV [15] for the first two and 0.32 eV [17, 22] for the latter.

TABLE I. Parameters of effective mass normalized by m_e , band gap [23], and SOC, *Dresselhaus* [18] and *Rashba* [22] for GaAs, GaSb, and InAs SCs.

	GaAs	GaSb	InAs
m_j^*/m_e	0.067	0.041	0.023
E_g (eV)	1.519	0.810	0.418
γ ($\text{eV} \text{ \AA}^3$)	27.6^a	187	130
α ($\text{eV} \text{ \AA}$)	0.0873	0.3	1.01

^a Ref. [15].

In equation (10), the term $R_{\alpha} = (2m_b^*\alpha/\hbar^2)k_{\parallel}\sin(2\phi_l)$ related to the *Rashba* SOC does not generate any change to the electron wave vector within the potential barrier, because the term $R_{\alpha} = 0$ when $\phi_l = 0$ ($\theta_0 = \theta_m$) or $R_{\alpha} \ll 1$ when $\phi_l = \pi/4$, for the values of α from table I.

Similarly, the *Dresselhaus* SOC does not generate significant changes in the TMR, as can be seen in Fig. 5. However, a decrease in the TMR for the Fe/SC/Fe PSVs is observed when the SOC constant changes from 0 to α , reaching its maximum value when ϕ_l is equal to $\theta_m = \pi/4$.

On the other hand, in Fig. 5, a comparison of the TMR calculated by the conductance defined in equations (15) and (16) as a function of the direction of \mathbf{n}_l is shown. It can be observed that the TMR by LBA is slightly lower at $\theta_l = \theta_m$ compared to that calculated by the conductance G_{ℓ} , making it a good approximation. Additionally, it can be seen that the PSV with the best theoretical performance is Fe/GaSb/Fe, followed by Fe/InAs/Fe, and finally Fe/GaAs/Fe.

In Fig. 6, a comparison of the TMR calculated by the conductances G_{ℓ} and G_{ℓ}^v (LBA) is also presented as a function of the thickness of the SC, where it can

be seen that if $\theta_l = \pi/4$, the performance for the PSV is maintained for $a \geq 3 \text{ nm}$ with a rapid convergence for the Fe/GaSb/Fe and Fe/GaAs/Fe trilayers, while for $1 \leq a < 3 \text{ nm}$, the Fe/GaAs/Fe PSV is more efficient than Fe/InAs/Fe. In the case $\theta_l = 0$, the TMR decreases significantly for the Fe/SC/Fe trilayer under study, because in this direction, the magnetization axis is not favored; a weak magnetization is present. Similarly, the efficiency among the PSVs remains within the described ranges.

Finally, when comparing the physical-mathematical model described in this article with the work *K. Kondo* [15], in which \mathbf{n}_j moves in the $y-z$ plane and \mathbf{n}_l is parallel to the y axis, which can be modeled as a particular case where $\theta_m = 0$, where the parallel and antiparallel states between \mathbf{n}_l and \mathbf{n}_r would be 0 and π radians, respectively. Under this assumption, in Fig. 7, there is no negative TMR even when considering the *Dresselhaus* SOC for the Fe/GaAs/Fe PSV, generating the first discrepancy with the aforementioned work; where the TMR converges to -60% starting at $a = 0.75 \text{ nm}$ when considering the *Dresselhaus* SOC, a result supported regarding the negative sign, but not the numerical value, by the work of M. Zenger et al. [16] but using a magnetic field of around 0.1 T and a voltage of 5 mV. Effects not taken into account in the work under analysis or in the present development. Additionally, it is observed that the TMR saturates at approximately 19.54%, with $\gamma = 0$ or $\gamma = 27.6 \text{ eV} \cdot \text{\AA}^3$. This value does not coincide with the result of *K. Kondo* [15]; except for $\gamma = 0$, where the convergence is similar.

Additionally, in the study under analysis, the Fe/GaSb/Fe trilayer converges to a TMR of 140% starting at $a = 2.5 \text{ nm}$, a result that does not coincide with the proposed model since for that thickness, the TMR is approximately 25.57% (see Fig. 8) due to the contribution of the *Dresselhaus* SOC.

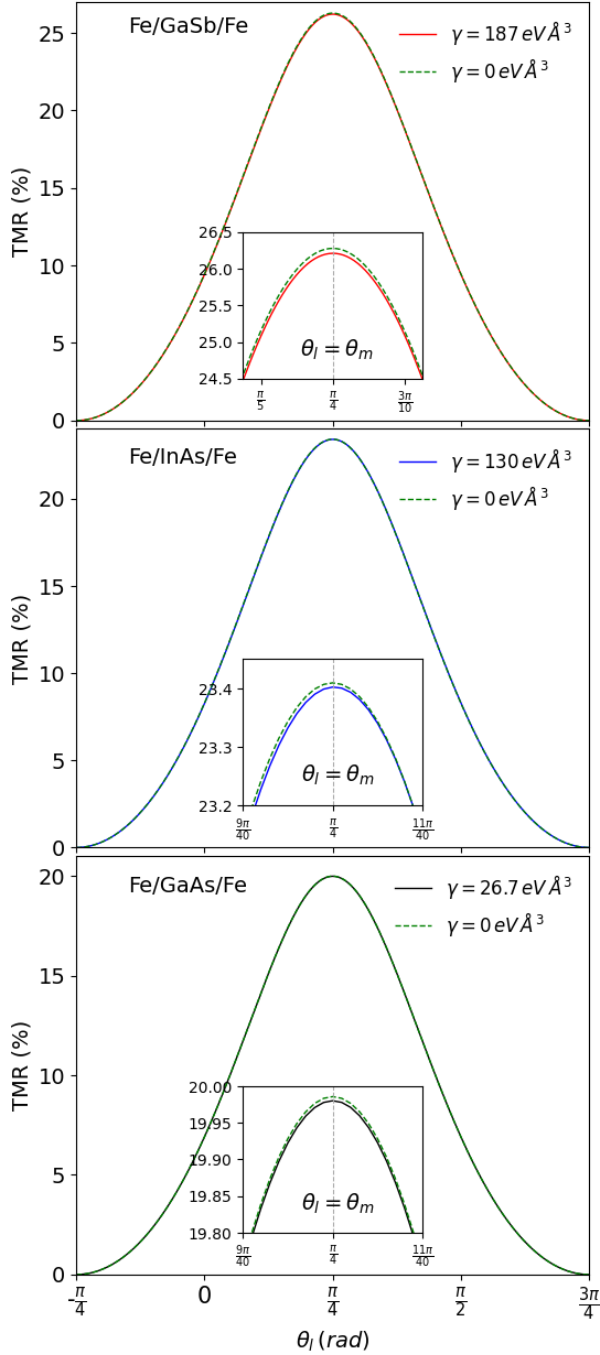


FIG. 5. Representation of the TMR for the Fe/SC/Fe PSVs as a function of the direction of \mathbf{n}_l . Where $a = 4$ nm, $\theta_m = \pi/4$, $\Delta_j = 3.46$ eV, and $E_F = 2.48$ eV. For GaSb and GaAs SCs, $V_0 = 0.75$ eV, and for InAs SC, $V_0 = 0.32$ eV.

IV. CONCLUSIONS

In relation to the above, for the physical-mathematical model proposed in this work, it is not observed that the *Rashba* SOC contributes to the TMR, while the *Dresselhaus* SOC is not so significantly. On the other hand, it is

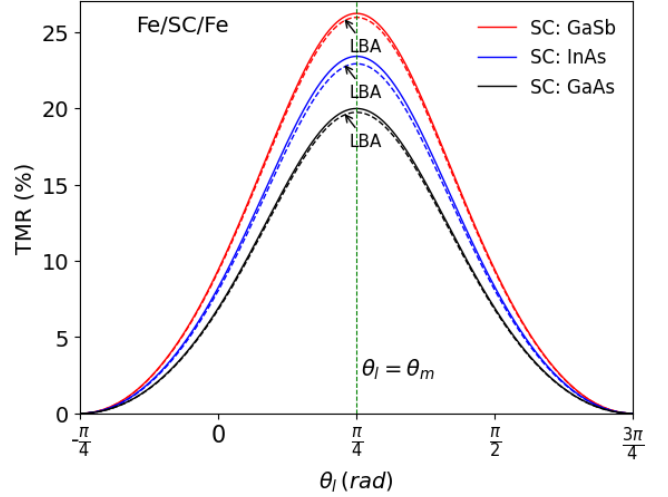


FIG. 6. Comparison of the TMR using the conductances G_ℓ and G_ℓ^v as a function of the direction of \mathbf{n}_l for a Fe/SC/Fe-type PSV where $a = 4$ nm, $\theta_m = \pi/4$, $\Delta_j = 3.46$ eV, $E_F = 2.48$ eV, and $k_{\parallel j} = k_{\parallel \sigma} = 0.2$ nm $^{-1}$ for the LBA case. For GaSb and GaAs SCs, $V_0 = 0.75$ eV, and for InAs SC, $V_0 = 0.32$ eV.

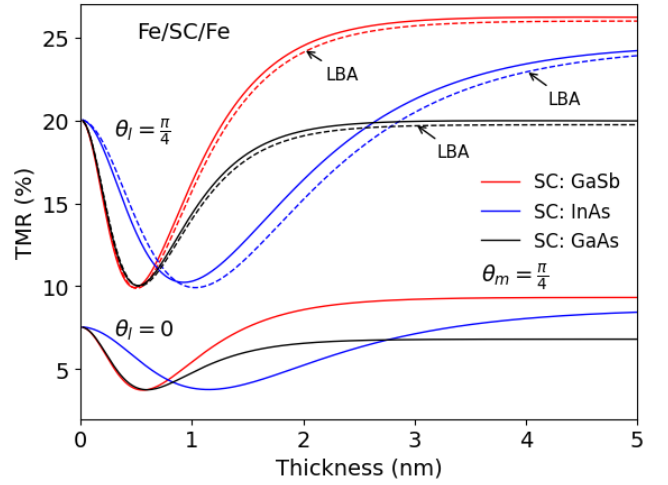


FIG. 7. Comparison of the TMR using the conductances G_ℓ and G_ℓ^v as a function of the thickness of the SC for a Fe/SC/Fe-type PSV where $\Delta_j = 3.46$ eV, $E_F = 2.48$ eV, and $k_{\parallel j} = k_{\parallel \sigma} = 0.2$ nm $^{-1}$. For GaSb and GaAs SCs, $V_0 = 0.75$ eV, and for InAs SC, $V_0 = 0.32$ eV.

observed that the direction of the magnetization normal vector directly influences the magnitude of the TMR, as it maximizes it when parallel to the crystallographic axis that favors magnetization.

Finally, the TMR results for Fe/SC/Fe-type PSVs with GaAs and GaSb SCs do not agree with those presented by *K. Kondo* [15].

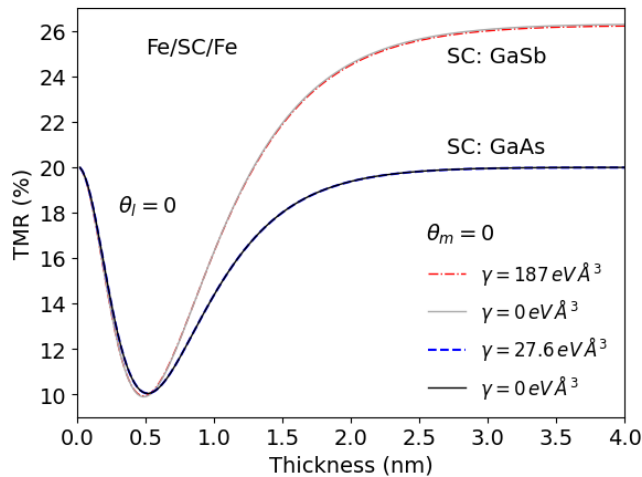


FIG. 8. TMR calculated with the conductances G_ℓ as a function of the thickness of the SC, considering the Fe/SC/Fe trilayer where $\theta_m = 0$, $\Delta_j = 3.46$ eV, $E_F = 2.48$ eV, and $k_{\parallel j} = k_{\parallel \sigma} = 0.2$ nm $^{-1}$. For GaSb and GaAs SCs, $V_0 = 0.75$ eV, and for InAs SC, $V_0 = 0.32$ eV.

ACKNOWLEDGMENTS

The authors would like to thank the Master's Program in Physical Engineering of the Facultad de Ciencias Naturales, Exactas y de la Educación of the Universidad del Cauca, Colombia, and the Instituto de Física La Plata (CONICET) Argentina, for providing the space and time for the development of this work.

-
- [1] M. Kumar Yadav and S. Kumar Gupta, *Micro and Nanostruc.* **165**, 207192/1 (2022).
- [2] K. Takase, L. Duc Anh, K. Takiguchi, and M. Tanaka, *Appl. Phys. Lett.* **117**, 092402/1 (2020).
- [3] M. Gani, K. A. Shah, S. A. Parah, and P. Misra, *Phys. Lett. A* **384**, 126171/1 (2020).
- [4] T. Kubota, Z. Wen, and K. Takanashi, *J. Magn. Magn. Mater.* **492**, 165667/1 (2019).
- [5] Y. C. Tao, J. G. Hu, and H. Liu, *J. Appl. Phys.* **96**, 498 (2004).
- [6] J. E. Bunder, *Appl. Phys. Lett.* **91**, 092111/1 (2007).
- [7] A. Saffarzadeh and A. A. Shokri, *J. Magn. Magn. Mater.* **305**, 141 (2006).
- [8] A. A. Shokri, *Eur. Phys. J. B* **50**, 475 (2006).
- [9] E. N. Economou and C. M. Soukoulis, *Phys. Rev. Lett.* **46**, 618 (1981).
- [10] J. C. Slonczewski, *Phys. Rev. B* **39**, 6995 (1989).
- [11] Y. Qi, D. Y. Xing, and J. Dong, *Phys. Rev. B* **55**, 2783 (1998).
- [12] X. Yang, R. Y. Gu, D. Y. Xing, Z. D. Wand, and Jinming-Dong, *Int. J. Mod. Phys. B* **11**, 3375 (1997).
- [13] S. Ju, T.-Y. Y. Cai, G.-Y. Guo, and Z.-Y. Li, *J. Appl. Phys.* **104**, 053904/1 (2008).
- [14] A. Matos-Abiague and J. Fabian, *Phys. Rev. B* **79**, 155303/1 (2009).
- [15] K. Kondo, *J. Appl. Phys.* **111**, 07C713/1 (2012).
- [16] M. Zenger, J. Moser, W. Wegscheider, and D. Weiss, *J. Appl. Phys.* **96**, 2400 (2004).
- [17] J.-D. Lu and J.-W. Li, *Appl. Surf. Sci.* **256**, 4027 (2010).
- [18] V. I. Perel', T. S. A., I. N. Yassievich, S. D. Ganichev, V. V. Belkov, and W. Prettl, *Phys. Rev. B* **67**, 201304/1 (2003).
- [19] M. Wimmer, M. Lobenhofer, J. Moser, A. Matos-Abiague, D. Schuh, W. Wegscheider, J. Fabian, K. Richter, and D. Weiss, *Phys. Rev. B* **80**, 121301(R)/1 (2009).
- [20] D. K. Ferry and S. M. Goodnick, *Transport in Nanostructures*, 1st ed. (Cambridge University Press, 1997).
- [21] J. A. Zúñiga, *ACCEFYN* **47**, 785 (2023).
- [22] H. Dakhlaoui, M. Nefzi, N. S. Al-Shameri, A. A. Suwaidan, H. Elmobkey, S. Almansour, and I. Alnaim, *Physica B Condens. Matter* **597**, 412403/1 (2020).
- [23] J. Fabian, A. Matos-Abiague, C. Ertler, P. Stano, and I. Žutić, *Acta Phys. Slovaca* **57**, 1 (2007).
- [24] M. B. Stearns, *J. Magn. Magn. Mater.* **5**, 167 (1977).
- [25] G. Autès, J. Mathon, and A. Umerski, *Phys. Rev. B* **82**, 115212/1 (2010).